

## MATERIALS SCIENCE

Special Topic: Graphene—From basic science to useful technology

# Three-dimensional graphene networks: synthesis, properties and applications

Yanfeng Ma and Yongsheng Chen\*

## ABSTRACT

Recently, three-dimensional graphene/graphene oxide (GO) networks (3DGNs) in the form of foams, sponges and aerogels have attracted much attention. 3D structures provide graphene materials with high specific surface areas, large pore volumes, strong mechanical strengths and fast mass and electron transport, owing to the combination of the 3D porous structures and the excellent intrinsic properties of graphene. This review focuses on the latest advances in the preparation, properties and potential applications of 3D micro-/nano-architectures made of graphene/GO-based networks, with emphasis on graphene foams and sponges.

**Keywords:** graphene, graphene oxide, three-dimensional network, graphene foam, graphene sponge, graphene aerogel

## INTRODUCTION

Graphene has many unique and excellent properties, such as its electronic properties, associated with its unique gapless conical band structure, its high mechanical strength, flexibility, thermal conductivity and stability, and its efficient wide range of light absorption. These properties have made graphene a promising candidate for a broad range of applications in many fields [1–3]. It is hoped that graphene, in bulk or in composite materials, can preserve its extraordinary properties. However, the irreversible agglomeration or restacking of graphene sheets, because of the strong van der Waals interactions and high inter-sheet junction contact resistance between isolated graphene sheets, severely suppress the intrinsically high conductivity and mechanical strength of individual graphene sheets and diminish its accessible surface area.

Many efforts have been made to tackle this challenge. One effective way is to engineer a graphene material in which individual graphene sheets are bonded together to construct three-dimensional (3D) networks, avoiding re-stacking of individual graphene sheets. This is important for maintaining graphene's intrinsic properties in the bulk and

enhancing the use of graphene in practical applications. Tremendous efforts have been devoted to developing the synthesis and applications of 3D graphene networks (3DGNs) with various morphologies, structures and properties [4–7]. Typical 3DGNs reported in the literature include graphene foams (GFs), graphene sponges (GSs) and graphene aerogels (GAs). GFs were first synthesized using nickel foam as the template [8]. Thus, the GFs inherited the macroporous structure of the nickel foam, with a continuous and interconnected 3DGN. GSs have a similar porous structure to GFs, but the graphene sheets are partially oriented or aligned nearly parallel with each other, creating an anisotropic lamellar structure [9]. GSs are named for their highly efficient and recyclable absorption performance, similar to sponges [10]. GAs are usually produced using sol–gel chemistry, which involves reducing graphene oxide (GO) to form a highly cross-linked graphene hydrogel (GH), followed by freeze-drying or supercritical drying to remove the absorbed water [11, 12]. Although they have differences in their structures and properties, GFs, GSs and GAs all have excellent properties, such as a high surface area, high porosity, low density,

Key Laboratory of Functional Polymer Materials and the Centre of Nanoscale Science and Technology, Institute of Polymer Chemistry, College of Chemistry, Nankai University, Tianjin 300071, China

\*Corresponding author. E-mail: yschen99@nankai.edu.cn

Received 13 August 2014; Revised 5 October 2014;

Accepted 8 October 2014

high electric conductivity and good mechanical properties.

Until recently, a number of synthetic methods to fabricate 3DGNs, based on the strategies of either direct growth from a carbon source or by the assembly of GO/graphene sheets have been developed. The 3D structures provide graphene materials with high specific surface areas (SSA), strong mechanical strengths and fast mass and electron transport kinetics, owing to the combination of 3D porous structures and the excellent intrinsic properties of graphene. 3D structures can be used in many fields including use as absorbents, catalysis, sensors, and use in energy storage and conversion and biological applications. The synthesis routes and applications of 3DGNs have been summarized in detail in several specialized reviews with different emphasis [5–8]. Here, this review will focus on the latest advances in the preparation, properties and potential applications of 3D micro-/nano-architectures of graphene/GO-based networks, especially on GFs and GSs, in a more general view.

## SYNTHESIS

Several methods have been reported for fabricating 3DGNs. These methods have been classified according to the different points of view in the published reviews [4–7]. Here, they are grouped into two categories: one is the direct synthesis of 3DGNs from carbon sources such as methane, ethanol and sugar. The other is the assembly of GO or graphene sheets through a variety of ways.

### Direct synthesis of 3DGN

#### Template-assisted CVD growth

Chemical vapor deposition (CVD) is a convenient way to grow graphene with controlled layers and sizes. Based on the conventional CVD process for graphene growth, which uses flat metal substrates as catalysts, 3DGNs can be prepared by CVD using pre-fabricated 3D metal substrates (such as nickel foam) as the catalysts and templates [8, 13–16]. After etching off the nickel template, free-standing 3DGNs with controlled morphologies and properties can be obtained. Furthermore, by coating a nickel layer on a predefined substrate structure, for example nickel-coated pyrolyzed photoresist films [17], 3DGNs with the desired morphologies can also be produced. Along with the 3D metal substrates being used as the sacrificial template, other materials such as anodic aluminum oxide (AAO) [18], MgO [19], ZnO [20], metal nanostructures [20–23] and even metallic salts [24, 25] have also been used as templates to produce 3DGNs.

Cheng and his group first reported the synthesis of 3D GFs using nickel foam as the template using CVD [8]. By pyrolyzing  $\text{CH}_4$  at  $1000^\circ\text{C}$  under ambient pressure at a constant rate in the presence of nickel foam with an interconnected 3D macroporous structure, three-layered graphene films were precipitated on the surfaces of the nickel foam. Then, a thin layer of polymethyl methacrylate (PMMA) was deposited on the surfaces of the graphene films to protect the graphene network, followed by etching the nickel skeleton in an HCl (or  $\text{FeCl}_3$ ) solution. By using hot acetone to remove the PMMA layer, a free-standing GF was obtained. The resultant GF monoliths exhibited a continuous and interconnected 3DGN in which all of the graphene sheets were in direct contact with each other, without any breaks, inheriting the interconnected 3D framework from the nickel foam template. The surface area of the 3DGNs was dependent on the number of layers in the graphene film, which could be as high as  $850\text{ m}^2/\text{g}$  for 3DGNs made of a three-layer graphene film. Importantly, the 3DGNs also exhibited unique properties in their electrical conductivity, mechanical strength [8, 13, 14] and thermal conductivity [15]. GFs with monolayer graphene sheets were also prepared using Cu foam as the template. However, a free-standing sheet could not be obtained because monolayer graphene cannot bear the liquid capillary force caused by the evaporation of acetone.

Similar high-quality 3DGNs have been achieved by other groups using different carbon sources and/or different conditions [26–30]. Zhang's group showed that 3DGNs could be produced with an atmospheric pressure CVD process using ethanol as the carbon source [26]. By soaking nickel foam in an asphalt–toluene solution and then placing it in a furnace under an  $\text{Ar-H}_2$  flow at  $940^\circ\text{C}$  for 10 min, Li and coworkers synthesized GFs [27].

Ruoff and coworkers [31] explored the effect of different etching agents for removing Ni, on the thickness of the 3D GFs. They found that the Ni etching processes, using ferric nitrate ( $\text{Fe}(\text{NO}_3)_3$ ) and ammonium persulfate ( $(\text{NH}_4)_2\text{S}_2\text{O}_8$ ), were much slower and gentler than using diluted HCl. This is helpful for controlling the density of the resulting 3DGNs, which is ultimately critical for the temperature-dependent electron and phonon transport in these materials.

A Ni foam/sponge-template-assisted-CVD process is an effective way to produce 3DGNs with controlled morphologies. However, as the GF inherited the structure of the nickel foam template, which usually has a pore size of hundreds of micrometers in diameter, the obtained GF possessed large pore sizes with a high porosity (about 99.7%) [8]. To obtain GF with a pore size on the scale of

micro- or nanometers, other template precursors have been explored.

Zhou *et al.* [18] reported the growth of 3D graphene on porous  $\text{Al}_2\text{O}_3$  ceramics using CVD. The AAO template is a regular 1D channel array with an average pore size of  $\approx 95$  nm and a pore center-to-center distance of  $\approx 125$  nm, after firing at  $1200^\circ\text{C}$  for 2 h. Graphene was grown at  $1200^\circ\text{C}$  for 30 min under the flow of  $\text{Ar}:\text{H}_2:\text{CH}_4 = 450:50:10$  sccm. Bilayer graphene sheets grew around the surfaces of the AAO channel. The graphene/ $\text{Al}_2\text{O}_3$  composite contained an interconnected macroporous graphene framework with low sheet electrical resistance, down to  $0.11 \Omega/\text{sq}$ , and a thermal conductivity of  $8.28 \text{ W}/(\text{m K})$ .

Wei and his group [19] produced 3D graphene with nanomeshes by using porous MgO layers as the template. After introducing methane for the CVD growth of graphene, one to two graphene layers were formed on the MgO surfaces. The graphene nanomeshes had large SSAs up to  $1654 \text{ m}^2/\text{g}$  with pore diameters around 10 nm.

Chen and coworkers [23] developed a nanoporous Ni-based CVD technique to grow high-quality 3D nanoporous graphene sheets with tunable pore sizes from ca. 100 nm to ca.  $2.0 \mu\text{m}$ , as well as coherent quantum electronic properties in the interconnected 3D structures. A nanoporous Ni (np-Ni) substrate with a thickness of ca.  $30 \mu\text{m}$  and an average nanopore size of ca. 10 nm was prepared by electrochemically leaching Mn from a  $\text{Ni}_{30}\text{Mn}_{70}$  precursor in a weak acidic solution. The as-prepared np-Ni was annealed at  $900^\circ\text{C}$  for 5–30 min in a CVD system under a mixed atmosphere of  $\text{H}_2$ , Ar and benzene. Graphene films uniformly grew on the surfaces of the nanosized Ni ligaments and the pore size of the graphene could be tailored from 100 nm to  $2.0 \mu\text{m}$  by controlling the CVD time and temperature.

A nickel salt ( $\text{NiCl}_2 \cdot 6\text{H}_2\text{O}$ ) has also been used both as a catalyst and a template precursor to synthesize GFs [25]. The first step was to anneal  $\text{NiCl}_2 \cdot 6\text{H}_2\text{O}$  at  $600^\circ\text{C}$  to form a 3D Ni skeleton. In this process,  $\text{NiCl}_2 \cdot 6\text{H}_2\text{O}$  was first flowed through a  $\text{H}_2$ -Ar mixed gas and then treated with a mixture of water vapor and hydrogen chloride. The subsequent procedure was CVD growth, operated at  $1000^\circ\text{C}$ , followed by etching the Ni. A 3D graphene macroscopic network was obtained. The pore size of the 3DGN was several micrometers, with a relatively high density ranging from 22 to  $100 \text{ mg}/\text{cm}^3$ , compared with that of the Ni foam ( $1 \text{ mg}/\text{cm}^3$ ) [8].

### Non-template approach

Along with the template-assisted CVD method, non-template approaches to directly synthesize

3DGNs have also been reported [32–35]. Chen's group [32–34] developed a direct current plasma-enhanced CVD approach to directly grow vertical graphene sheets on various conductive substrates, including Au and stainless steel, using  $\text{CH}_4$  as the carbon source. The graphene sheets firmly adhered to the substrates with many active sites at the edges of the sheets and connected with each other forming 3D porous graphene, making them suitable for sensing applications. Recently, inspired by an ancient food art of 'blown sugar', Wang and coworkers developed a technique to grow a 3D self-supported graphene bubble network [35]. This foam-like architecture was packed full of large polyhedral bubbles with an average diameter of  $186 \mu\text{m}$ . A typical synthesis procedure is as follows: 10 g of glucose was mixed with 10 g of ammonium salt ( $\text{NH}_4\text{Cl}$ ), which was then heated at a rate of  $4^\circ\text{C}/\text{min}$ . Then it was treated at  $1350^\circ\text{C}$  for 3 h under an Ar atmosphere in a tube furnace. A black foam-like 3D graphene bubble network was obtained. The bubble network consisted of either mono- or few-layered graphitic membranes that were tightly glued, rigidly fixed and spatially scaffolded by micrometer-scale graphitic struts. Such a topological configuration provides intimate structural interconnectivities, a freeway for electrons/phonons to transport, a huge accessible surface area as well as robust mechanical properties. This approach is a general path to synthesize 3D graphene analogs.

### Assembly of GO sheets

The assembly of 2D GO/graphene sheets to form 3DGNs begins by dispersing GO in a solution. In a GO solution, there is a force balance between the van der Waals attractions from the basal planes and the electrostatic repulsions from the functional groups of the GO sheets [4]. Once the balance is broken (for instance by changing the pH of the GO dispersion solution [36]), adding cross-linkers [37] or ultrasonication of the GO dispersion solution [38] causes gelation to occur. In a typical procedure, GO sheets are first dispersed in a solution and then through a series of procedures, involving gelation and reduction processes, followed by special drying techniques, 3DGNs are obtained with the graphene sheets. They are either physically or chemically linked to each other.

A variety of methods based on this strategy have been developed, including chemical reduction [39, 40], electrochemical reduction [41, 42], hydrothermal processes [43–48], metal ion-induced self-assembly [49], flow-directed assembly, [50] evaporation-induced self-assembly [51], the Langmuir-Blodgett technique [52], layer-by-layer

deposition [53] and a nucleate boiling method [54] for GO dispersions. Apart from these, to suppress the restacking of the graphene sheets during assembly, a functionalization-lyophilization-microwave treatment was designed, and ultralight GAs with excellent elasticity were produced [55].

As this strategy has already been thoroughly summarized and analyzed [4–7], in the following, we will focus on several typical techniques and on latest advances in this field.

### Self-assembly of GO through chemical, electrochemical or hydrothermal reduction

GHs and GAs could be produced via the simple chemical reduction of a GO aqueous dispersion [39, 40]. Sodium ascorbate,  $\text{NaHSO}_2$ ,  $\text{Na}_2\text{S}$ , Vitamin C, hydrogen iodide or hydroquinone could be used as the reducing agent. A reducing agent is typically added to aqueous suspensions containing GO and heated to 90–95°C for a certain period of time (30 min–3 h). Then, GHs and GAs can be obtained after removing the residual inorganic compounds and absorbed water, respectively. The mechanical properties of GHs are comparable to those of chemically cross-linked polymer hydrogels. The bulk electrical conductivity of the GA was around 1 S/cm, similar to a GA prepared by organic sol–gel chemistry combined with pyrolysis.

Electrochemical reduction is usually used to directly fabricate 3D graphene-based electrodes [41, 42]. The typical procedure is to electrochemically reduce GO on metal electrodes (e.g. Au) in a 3 mg/ml aqueous GO suspension containing 0.1 M lithium perchlorate ( $\text{LiClO}_4$ ) at an applied potential of  $-1.2$  V (vs saturated calomel electrode) for 10 s. During this process, GO sheets were deposited on the surfaces of the electrodes and assembled into 3D interpenetrating networks and at the same time they were reduced to conductive reduced GO (RGO).

Hydrothermal reductions have been widely used to reduce GO and induce the self-assembly of GO, using an autoclave at moderately high temperatures (90–200°C) and elevated solution pressures. 3DGNs have been produced through hydrothermal processing [43–48]. GHs with high electrical conductivity have been fabricated via a one-step hydrothermal process [43]. They were easily produced by heating a 2 mg/ml GO aqueous dispersion sealed in a Teflon-lined autoclave at 18°C for 12 h. After freeze-drying, the resultant hydrogels had well-defined and physically interconnected 3D porous networks. They had a relatively high electrical conductivity ( $5 \times 10^{-3}$  S/cm) from the recovery of the  $\pi$ -conjugated system of GO sheets upon hydrothermal reduction.

### Freeze-drying/Freeze-casting

Generally, a drying procedure should be applied after gelation and reduction of the GO dispersion to remove any water and organic molecules from the pores in the 3DGNs. The most commonly used drying technique is freeze-drying/freeze-casting, as it is the most convenient and efficient way to remove absorbed molecules without destroying the 3D graphene framework.

Freeze-drying is a versatile method, used to prepare GAs from GHs. Mechanically strong and electrically conductive GAs can be prepared by either supercritical drying or freeze-drying hydrogel precursors [11]. Hydrogel precursors have been obtained by mixing uniformly quantitative L-ascorbic acid (AA) with an aqueous GO suspension and then heating the mixture without stirring for 2 h. GAs have been obtained by forming physical cross-links between graphene sheets using sol–gel chemistry. Sol–gel chemistry involves reducing GO to form highly cross-linked hydrogels, which can then be freeze-dried or supercritical- $\text{CO}_2$ -dried to form GAs.

GSs could be produced through a hydrothermal process followed by freeze-drying/freeze-casting. Sun and coworkers fabricated GSs by the self-assembly of GO solutions with hydrothermal reductions and freeze-drying [10]. By changing the parameters during freeze-casting, especially the freezing temperature, the porous microstructures of GSs can be controlled (Fig. 2) [9]. With this route, 0.5 ml ammonia (30 v/v%) was added to a homogeneous GO (60 mg) colloidal dispersion (20 ml) to tune the pH value to 10. The GO dispersion was then transferred into a sealed reactor and heated to 180°C for 20 h and then a RGO gel block was obtained. The RGO block was placed in a cold source at a constant temperature. The rate of crystal growth was controlled by regulating the temperature of the cold source. Freezing lasted for several minutes, until the gel block was fully solidified. After the gel was completely frozen, the samples were placed in a freeze-dryer for 48 h, generating black GSs.

### Assembly of GO on conductive substrates

Inspired by the recent findings on GO being directly reduced by active metals (such as Al, Fe and Cu), a new method of substrate-assisted reduction and the assembly of GO for the spontaneous formation of 3D graphene structures on arbitrary conductive substrates was developed [56]. These graphene assemblies include microtubes, four-way pipes, spiral tubes, multi-channel networks and micropatterns. The substrates containing the active metals Zn, Fe and Cu, the inert metals Ag, Pt and Au, a

semiconducting Si wafer, a non-metallic carbon-based film and even indium-tin oxide (ITO) have been readily achieved without any additional reducing agents.

Taking the active metal Cu foil as an example, when a Cu foil was immersed in an aqueous 1 mg/ml GO suspension with a pH of 4.0 for several hours without any additives, a black layer of RGO covered the whole surface, which was composed of a 3D network of RGO sheets. The reduction of GO and the oxidation of the metal substrates are associated with GO gaining electrons and the metal losing electrons. For inert metals or other conductive surfaces, by simply supporting them on an active metal substrate, GO could be reduced and deposited on the surfaces via a process in which the inert conductive substrate acts as a cathode to reduce GO and to deposit RGO from the suspension, while the active metal foil serves as an anode, where the metal is oxidized.

#### Template-assisted assembly

Alternatively, 3D graphene architectures can be fabricated by assembling GO/graphene sheets on the surfaces of the templates through electrophoretic deposition, dip-coating, refluxing in an autoclave and template-assisted freeze-drying [4]. Apart from the nickel foams used in the CVD method, spherical materials such as polystyrene (PS) balls [57] and silica nanoparticles (NPs) [58], skeleton materials including commercially available sponges [59], Nafion scaffolds [60] and textile fibers [61] can also be used as templates.

Free-standing 3D macroporous graphene films have been fabricated with PS spheres (2.0  $\mu\text{m}$ ) as the template [57]. First, a negatively charged chemically modified graphene (CMG) colloid and a positively charged PS suspension were prepared separately. Then they were mixed and dispersed in a solution under a controlled pH ( $\approx 2$ ), where the two compounds had the same surface charges. When the pH was increased to 6, CMGs and PS spheres assembled because of the electrostatic interactions and hydrophobic characteristics between them. These were subsequently integrated into PS/CMG composite films through a filtering process. The PS particles in the PS/CMG composite films were selectively removed using toluene, leaving behind an open porous structure. The porous structure did not collapse after the PS template was removed because of the interconnected nature of the multilayered CMG walls in the assembled 3D structures. The well-defined interconnected pore networks of the embossed-CMG films also had a high electrical conductivity (1204 S/m).

#### Assembly using cross-linkers

Adding a cross-linker to the GO dispersion functionalized the graphene surfaces and improved the interactions between the GO/graphene sheets. The first cross-linker reported was polyvinyl alcohol (PVA) [37], which promoted the gelation process of a GO dispersion to form 3D graphene structures. Thereafter, many materials have been used in literature as cross-linkers to assemble GO sheets, such as DNA [62], metal ions [49], polymers [63], amines [64, 65] and organic molecules [66, 67].

Qu and coworkers used pyrrole (Py) as a cross-linker to produce GSs [67]. Using this approach, the nitrogen-rich molecules were able to interact with the GO sheets through hydrogen bonding and  $\pi-\pi$  interactions, strengthening the binding between the GO sheets and reducing the self-stacking of the GO during the hydrothermal reduction process. As a result, the sponge volume was 500% greater than that with only GO. Furthermore, polypyrrole (PPy) RGO sponges exhibited a high conductivity of 30 S/cm. Luan *et al.* [65] designed and fabricated 3D GO structures on the molecular level using different aromatic diamines such as *o*-phenylene diamine (oPDA) and *p*-phenylene diamine (pPDA) as the cross-linking agents. At the same GO concentration, the pPDA-GO hydrogels (GOHs) exhibited Brunauer–Emmett–Teller surface areas and pore volumes that were about twice as large as those of the oPDA-GOHs because of the longer amine-to-amine distance of pPDA. The adsorption capability of pPDA-GOH was five times higher than that of the graphene/carbon nanotubes (CNT) hybrid structure due to the well-developed 3D networks. Recently, Chen *et al.* [68] reported the template-free assembly of 3DGN hollow spheres, cross-linked by PVA fibers at the water/toluene interface. This method involved the formation of highly stable micron-sized Pickering emulsions by mildly sonicating the GO aqueous solution and toluene in the presence of PVA, followed by direct freeze-drying the mixture to preserve the unique 3D hollow spherical structures. The presence of PVA is critical for supporting the spherical GO structures and interconnecting the GO hollow spheres into stable 3D structures.

## PROPERTIES

Table 1 lists some of the physical properties of several typical samples of 3DGNs, including the SSA, electric conductivity, pore structure, density and mechanical properties. It shows that 3DGNs, especially GFs, GSs and GAs, possess excellent properties including large surface areas and pore volumes,

**Table 1.** Physical properties of several typical samples of 3DGNs, synthesized using different methods

No.	Synthesis method	Specific surface area (m <sup>2</sup> /g)	Pore structure	Density (mg/cm <sup>3</sup> )	Electrical conductivity (S/cm)	Mechanical property	Ref.
1	GF/Ni Foam template-assisted CVD growth	~850 (~3 Layer graphene)	Porosity ~99.7% Pore size ~400 μm	~5 (~3 Layer graphene)	~7 (~3 Layer graphene)	Flexible	[8]
2	GS/freezing drying of GH	53.4	Pore size 2–100 nm	9	0.54	Good Flexibility, Young's Moduli 7.56 kPa	[68]
3	GS/Self-assembly of GO, hydrothermal freeze-drying	423	Long axis ~570–620 μm short axis ~150–300 μm	12 ± 5			[10]
4	GA/supercritical drying or freeze drying of GH	512	Pore volumes 2.48 cm <sup>3</sup> /g, pore size 2–100 nm	12–96	~1	Young's moduli 1.2–6.2MPa	[11]
5	GA/organic cross-linker	584	Pore volume 2.96 cm <sup>3</sup> /g, pore size 1–100 nm	10	~1		[12]
6	GA/organic cross-linker		Porosity 99.7–99.8%	3–5		Highly compressible	[55]
7	GA/Chemical reduction			15	0.87		[39]
8	GH/hydrothermal		Pore size ~0.1–7 μm		$5 \times 10^{-3}$		[43]
9	3D RGO/hydrothermal freeze-drying			30	$2.5 \times 10^{-3}$	Compressive strength 0.042 MPa, compress modulus 0.26 MPa	[44]

low densities, good electrical conductivities and mechanical properties.

In general, 3DGNs with chemically bonded structures have better properties than physically assembled structures, such as a lower contact resistance, better conductivity, and they are stronger, tougher and more flexible. Table 1 shows that the bulk electrical conductivity of a chemically bonded GA is about 1 S/cm (Table 1, sample 5), more than two orders of magnitude greater than those reported for the macroscopic 3DGNs prepared with either physical cross-linkers alone or partial chemical bonding, for example, GO hydrogel having a conductivity of  $5 \times 10^{-3}$  S/cm (Table 1, sample 8) and 3D RGO having a conductivity of  $2.5 \times 10^{-3}$  S/cm (Table 1, sample 9). In comparison, GFs have a much higher electrical conductivity, owing to their unique continuous interconnected networks. The GAs had similar high electric conductivities of around 1 S/cm, both with and without an organic cross-linker. This may have been caused by cross-linking between the functional groups on the surfaces and edges of the GO during the sol-gel process.

Changes in the fabrication conditions caused differences in the structural features, such as the orientation and arrangement of the graphene sheets, the physical or chemical links between the graphene

sheets, the pore size and porosity and the number of layers of graphene sheets, changing their properties. The orientations of the graphene sheets in GFs and GSs are different. In GFs, the graphene sheets have no orientation. Thus, GFs have an isotropic structure (see Figs 1b and 2e) and properties. Conversely, the graphene nanosheets in GSs are stacked in highly ordered film-like structures and these large graphene

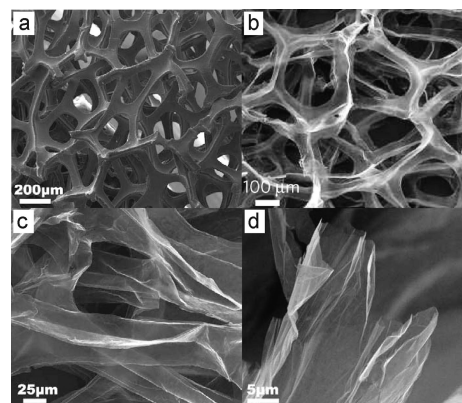


**Figure 1.** (a) Scanning electron microscope (SEM) image of an as-grown graphene film on the surface of a nickel foam. (b and c) SEM images of a free-standing GF and (d) the cross-sectional view [8].

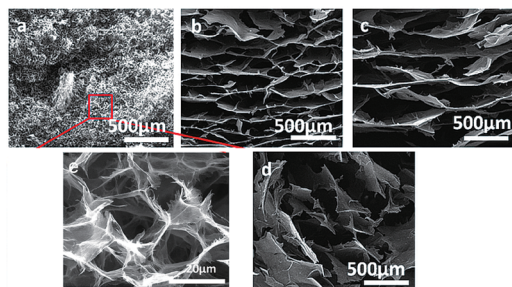


**Figure 2.** (a–d) SEM images of the porous structures of four 3DGNs fabricated at different freezing temperatures of  $-170$ ,  $-40$ ,  $-20$  and  $-10^{\circ}\text{C}$ , respectively. (e) Enlargement of the square area in image (a) [9].

films are aligned nearly parallel with each other, creating an anisotropic structure (see Figs 2b and 3a).

The preparation process for GFs is very versatile and can control both the macrostructure and microstructure [8]. The pore size and porosity can be tuned by changing the pore structure of the Ni foam. The average number of graphene layers, SSA and density of GFs can be controlled by changing the  $\text{CH}_4$  concentration. A higher  $\text{CH}_4$  concentration led to an increase in the number of graphene layers, and consequently large changes in the SSA, density and electrical conductivity of the GFs. The thickness and mass of the GFs increased as the number of graphene layers increased, while the density and SSA decreased with an increasing number of layers. The reason for the decrease in the density with an

increase in the number of graphene layers may have caused the framework to shrink and the HCl and acetone etching reduced with an increase in the thickness of the GFs. The electrical conductivity of the GFs first increased and then decreased as the number of graphene layers increased.

The microstructure and properties of GSs can be tuned by adjusting the synthesis conditions. When producing GSs by freeze-drying GH [9], the freezing temperature is critical. Both the pore size and pore wall thickness decreased over a wide range of 80 and 4000 times, respectively, as the freezing temperature decreased from  $-10$  to  $-170^{\circ}\text{C}$ . The pore morphology changed dramatically from anisotropic lamellar to uniform cellular structures. The Young's Modulus of the sponge could also be varied by 15 times (from 13.7 to 204.4 kPa). The mean pore size determines the water absorption properties of a GS. When the pore size was larger than  $300\ \mu\text{m}$ , the sponge was water resistant. When the pore size was smaller than  $150\ \mu\text{m}$ , the sponge could absorb water. When the pore size was between 150 and  $300\ \mu\text{m}$ , some areas near the center of the sponge were water absorbent, whereas the edges were water resistant. Water-absorbent GSs may be useful as electrodes in ionic liquids, whereas water-resistant GSs could be applied as oil absorbers. The properties of GSs could be regulated by controlling the freezing temperature, depending on what it is being used for.

## APPLICATIONS

3DGNs are composed of GO/graphene sheets. Thus, they inherit the excellent properties and wide range of applications of GO/graphene. Furthermore, as the shortcomings of GO/graphene have been overcome, at least partially, by constructing into 3D networks, 3DGNs show more excellent performance in practical applications.

### Catalysts

GO/graphene has been found to have potential catalytic properties in some reactions [69–71], including the hydration of alkynes, oxidation, oxidative coupling, Friedel–Crafts addition, aza-Michael addition, polymerization and photo-oxidation. Also, GO/graphene can be used as a catalyst support in many reactions, such as Suzuki–Miyaura coupling [72] and photocatalysis [73], owing to its 2D structure, large surface area, extraordinary electronic and mechanical properties and the abundant functional groups on the GO surfaces that provide many favorable sites where functional nanocomponents can anchor [70, 71]. Graphene-based catalysts can be used in organic synthesis, sensors, environmental

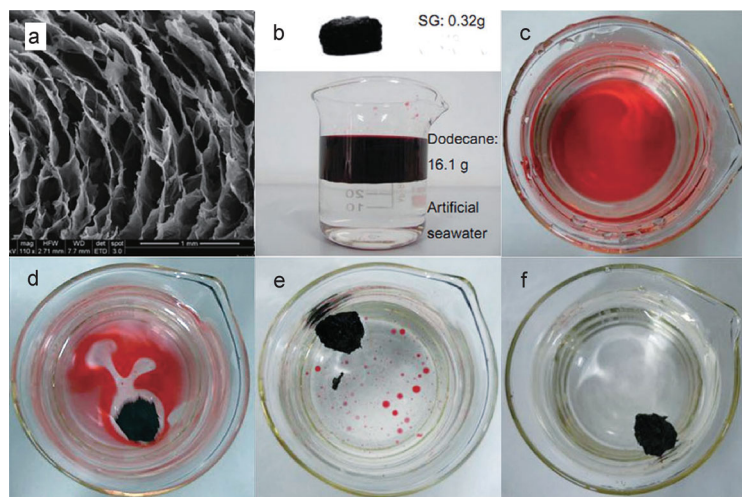


**Figure 3.** SEM image and oil absorption of a spongy graphene (SG), RGO sponge. (a) SEM image of the microporous structure of a RGO sponge. (b) Efficiency of oil absorption. A RGO sponge can be molded into any shape. The bulk of a RGO sponge with the shape of a triangular prism was obtained, with a mass of 0.32 g. This block absorbed 16.1 g of dodecane floating on water, corresponding to a weight gain of 50.3 g/g. (c–f) Absorption of dodecane in RGO sponge at intervals of 20 s. All of the dodecane (stained with Sudan red 5B) floating on artificial seawater was completely absorbed within 80 s [10].

protection and energy-related systems. However, the large resistance from structural defects and the strong planar stacking of graphene sheets lead to drastic deterioration of the properties. These shortcomings can be overcome by forming 3D graphene skeletons. The porous interconnected network is beneficial for ion diffusion and transfer kinetics, and provides a special reaction microenvironment and conductively multiplexed pathways for rapid charge transfer and conduction [7]. 3D GO/GNs are promising for use as either metal-free catalysts or robust matrices for accommodating metals, metal oxides and catalyst precursors for applications in many catalytic systems.

### 3DGNs as metal-free catalysts

In recent years, oxidative desulfurization has become a promising and emerging alternative to the conventional hydrodesulfurization technology used by most oil refineries around the world. Marques and coworkers [74] used 3D GO foams (GOFs) as catalysts to oxidize thioanisole. The GOFs were fabricated by hydrothermal treatment of an aqueous suspension of GO at 180°C for 12 h. The 3D GO catalysts had high catalytic activities (>90%) for the oxidation of thioanisole. This performed better than 2D GO and other metal-free catalysts such as fullerenes, periodic mesoporous silicas and cyclodextrins. Furthermore, the dosage of 3D GO was very low, around 11 wt% relative to the substrate. This is much lower than the 2D GOs usually found in the literature. More importantly, reactions catalyzed by 3D GO can be performed at room temperature. Thus, using 3D GO as a catalyst has many advantages, since it is a simple, metal-free and inexpensive catalyst. In addition, it can be recovered from the reaction media and subsequently reutilized.

### Doped 3DGNs as metal-free catalysts

The electronic properties of 3DGNs can be modified by doping them with heteroatoms, such as S, P, B and N. This helps to extend their potential applications [44, 75, 76].

*Sulfur-doped graphene networks for oxygen reduction reactions (ORR).* The –C–S–C– configuration of sulfur in a carbon matrix has been suggested to be the active site for promoting ORR activity [75]. Recently, Tan's group [75] reported the ORR properties of 3D sulfur-doped graphene networks (3D S-GNs). 3D S-GNs were synthesized using an ion-exchange/activation combination method with a 732-type sulfonic acid ion-exchange resin as the carbon precursor. The 3D S-GNs exhibited higher electrocatalytic activity than sulfur-free 3D GNs and

sulfur-doped carbon nanocages. Because of their unique structure and composition, the 3D S-GNs exhibited a similar electrocatalytic activity, but superior stability and methanol tolerance to the commercial Pt/C catalyst for four-electron oxygen reductions in alkaline solutions.

*B, N-doped GF as a metal-free catalyst for ORR.* By modifying the CVD method reported by Cheng's group, Qu and coworkers successfully prepared a series of nitrogen (3.1 atom%), boron (2.1 atom%) doped GFs and GFs co-doped with nitrogen (4.5 atom%) and boron (3 atom%) (BN-GFs)[76]. They used them as electrocatalysts in ORR through electrochemical measurements. The results showed that N-doping significantly improved the electrocatalytic activity. The synergetic effect associated with B- and N-co-doping caused the 3D BN-GF electrodes to become active, performing slightly better than Pt–C/GC electrodes in terms of the reduction in the peak current. This was because, not only the isolated N and B atoms could act as active sites for ORR through charge transfer with neighboring C atoms but also the interaction between the adjacent N and B atoms could reduce the bandgap energy, further facilitating the ORR performance of the BN-GF electrodes. B- and N-co-doping could also significantly enhance the electroactive surface area.

### 3DGNs and heteroatoms-doped 3DGNs as catalyst supports

The 3D porous structures of the 3DGNs facilitate the mass transfer and maximize the accessibility to the catalyst surfaces. Thus, 3DGNs are suited to support catalyst active materials. The ease of catalyst separation, high turnover, low catalyst loading and recyclability could potentially render 3DGNs applicable to industrial settings [77–82].

Qi and coworkers synthesized a 3D graphene-based CdS/P25/GA using a one-step hydrothermal self-assembled approach and used it in photoelectrochemical hydrogen production from water reduction under sunlight [77]. As a new photocatalyst, CdS/P25/GA exhibited enhanced light absorption, improved photocurrent, extremely efficient charge separation properties and superior durability.

Hu and coworkers [82] designed a complex catalyst system of ternary Pt/PdCu nanoboxes anchored to 3D graphene sheets by a dual solvothermal process. The electrocatalytic activity of Pt/PdCu/3DGF for ethanol oxidation was not only significantly higher than those of pure Pt and PdCu electrodes but also had a roughly 4-fold improvement over the well-established commercial Pt/C catalysts.

## Absorbents

One of the important features of 3D GO/graphene structures is their large accessible SSAs, and thus they can effectively absorb organic and inorganic contaminants. Furthermore, 3DGNs can be easily separated from solution, making them convenient to collect and recyclable. Thus, GO/GFs and GSs can be used as super absorbers in environmental remediation to remove a range of organic contaminants and heavy metal ions with high efficiencies [7, 25, 83].

## Organic contaminants

There has been a growing need for recyclable absorbents that can remove organic pollutants or oil spills from water. GO/grapheme-based foams, sponges and hydrogels with high surface areas, uniform structures, chemical stability in organic solvents, the ability to withstand high temperatures, and highly hydrophobic and oleophilic surfaces have been demonstrated to be effective as absorbers for a wide variety of oils, alkanes, water soluble alcohols and organic solvents [7, 10, 67, 84–89].

Shi's group found that a GO/DNA composite hydrogel could efficiently extract and remove the model dye safranin O from water, with the loading capacity estimated to be 960 mg/g GO [85]. Sun and coworkers fabricated RGO sponges with a 430 m<sup>2</sup>/g surface area and used them to absorb a series of oils and organic solvents [10]. Fig. 3 shows the structure of a RGO sponge and how much dodecane (stained with Sudan red 5B) it could absorb. This RGO sponge was able to absorb 20–85 g of oil or organic solvent per gram of RGO.

## Metal ions

Heavy metal ions that cause water pollution are currently attracting much attention owing to their toxic effects on the health of humans and other organisms in the environment [83]. 3D GOFs have high surface areas and huge pore volumes, with GO sheets containing many functional groups on their surfaces, which can act as binding sites for the complexation of metal ions. Thus, GO is a suitable adsorbent to remove a wide range of heavy metal ions [25, 83, 90].

Lei *et al.* [90] synthesized 3D GOF/Fe<sub>3</sub>O<sub>4</sub> nanocomposites for the removal of Cr(IV), and the nanocomposites exhibited a very large surface area of 574.2 m<sup>2</sup>/g and a maximum absorption capacity of 258.6 mg/g. Zhang's group explored the effect of 3D GOFs as an absorbent to remove heavy metal ions [83]. The GOFs had a high surface area (578.4 m<sup>2</sup>/g) and abundant oxygen functional groups. The maximum adsorption capacity for Zn<sup>2+</sup> is 326.4 mg/g, which is much higher than that of most conventional adsorbents, such as

activated carbon (22.03 mg/g), CNT (43.66 mg/g), carbon foam (130.76 mg/g) and 2D GO sheets (246 mg/g). For the removal of other cationic heavy metals, such as Cd<sup>2+</sup>, Pb<sup>2+</sup> and Fe<sup>3+</sup>, the maximum adsorption capacities are 252.5, 381.3 and 587.6 mg/g, respectively.

## Sensors

3DGNs are efficient biosensors and gas-sensing devices owing to their low-mass densities, large surface areas, good mechanical stabilities and high electrical conductivities [6, 7, 13].

Yavari *et al.* [13] reported highly sensitive gas detectors using macroscopic 3D GF networks. The performances of GFs as the active material in sensing devices were evaluated by monitoring their change in resistance ( $\Delta R/R$ ) as a function of time in a chemiresistor with a four-probe configuration for different analyte concentrations. The  $\Delta R/R$  of the GF active layers decreased from ~30% for 1000 ppm to ~5% for 20 ppm of NH<sub>3</sub>, exhibiting an improved sensitivity relative to individual single-wall nanotube device and commercially available conducting polymer sensors. In addition to NH<sub>3</sub>, GF sensors exhibit high efficiencies for detecting NO<sub>2</sub> with a  $\Delta R/R$  of ~4% for 20 ppm NO<sub>2</sub>.

The 3D structures of GFs/GSs are also suitable for accommodating biomolecules, bacteria or even cells to resemble an *in vivo* 3D environment. For this purpose, Huang and coworkers prepared 3DGF/CuO nanoflower composites as monolithic free-standing 3D biosensors for the electrochemical detection of AA [91]. The 3D conductive structures of the GFs were favorable for current collection, mass transport and loading bioactive chemicals. CuO nanoflowers further increased the active surface area and catalyzed the redox of AA. Thus, all of these features give the 3DGF/CuO composites outstanding biosensing properties such as an ultrahigh sensitivity of 2.06 mA mM<sup>-1</sup> cm<sup>-2</sup> to AA at a response time of 3 s.

## Biological applications

Along with biosensors, 3DGNs also exhibit great potential in biomedical applications [92, 93]. The first study used 3DGFs as cell culture substrates for human bone marrow-derived mesenchymal stem cells (hMSCs) [92]. GFs maintain the hMSC viability and stimulate changes in the morphology and protein expression patterns, indicating that spontaneous osteogenic differentiation occurs without extrinsic biochemical inputs. Tang and Cheng's group [93] investigated the pro- and anti-inflammatory

responses of microglia in GF culturing systems. They found that GFs supported the growth of microglia and showed comparable biocompatibility with commercially available tissue culture PS. These results open up new opportunities for the use of 3DGNs in biomedical applications.

### Transparent conductive electrodes

Kim and coworkers reported GF-based transparent conductive electrodes for use in GaN-based blue light emitting diodes (LEDs) [94]. Fig. 4 shows the fabrication procedure. The transmittance of the GF at 438 nm was about 71%, and it was 95 and 75% for bilayer graphene and ITO (150 nm), respectively. The sheet resistance of the GF on a quartz substrate was 800  $\Omega$ /sq, which is lower compared with 2D graphene films (1500–3000  $\Omega$ /sq). The forward operating voltage and light output power at an injection current of 100 mA for GaN-based blue LEDs with GF-based transparent conductive electrodes were improved by about 26 and 14%, respectively.

### Energy storage and conversion

Because of the high conductivity of the interconnected networks, the 3D porous structure, high electrochemical stability and the promise of high elasticity and mechanical stability, 3DGNs are considered as attractive and competent materials for application in the fields of energy storage and conversion, including fuel cells, batteries, solar cells and supercapacitors [4–7, 95].

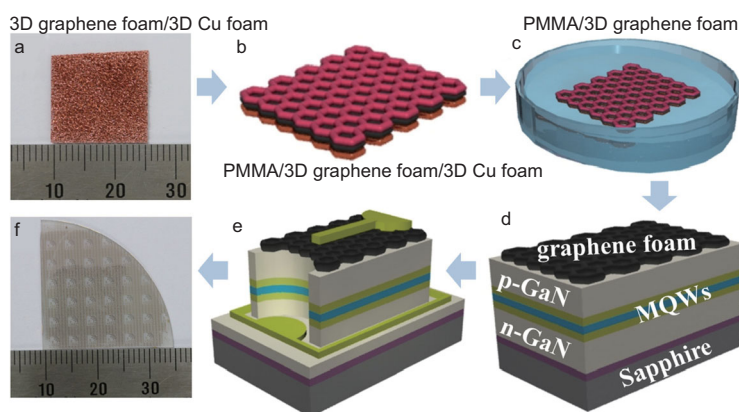


**Figure 4.** Fabrication processes of blue LED devices with GF-based transparent conductive electrodes. (a) A graphene film grown on Cu foam and (b) a GF-Cu foam spin-coated onto PMMA. (c) The Cu foam was etched by a 1 wt%  $(\text{NH}_4)_2\text{S}_2\text{O}_8$  solution. (d) After the PMMA-coated GF was transferred onto the p-GaN layer in the GaN-based blue LEDs, the PMMA layer was removed. (e and f) Blue LED devices were fabricated using standard photolithography processes. The structure of the shaded square-shaped area in (f) is the GF/LED/sapphire substrate. There was no GF outside the shaded square-shaped area [94]. MQW stands for multiple-quantum-well.

### Fuel cells

As described in the above, 3DGNs can be used either as catalysts or catalyst carrier supporting metals and alloys in oxidation and ORRs. In fuel cells, the role of 3DGNs is generally as a part of catalyst [75–82]. Yan's group [96] used GSs as the anode in microbial fuel cells (MFCs). The maximum power density reached was 427.0  $\text{W}/\text{m}^3$ , which is higher than that of the MFCs fabricated using carbon felt as the anode [96]. The macroporous structure of the GSs ensured that the microbes could easily diffuse and propagate inside the materials, resulting in a higher MFC performance.

### Batteries

Similar to 2D GO/graphene, 3DGNs have been used as active electrode materials in lithium-ion and lithium–sulfur (Li–S) batteries [4, 6, 14, 45, 97–100]. Fan and coworkers reported a bottom-up strategy, assisted by atomic layer deposition, to graft bicontinuous mesoporous nanostructured  $\text{Fe}_3\text{O}_4$  onto 3DGFs and directly used the composite as the lithium-ion battery anode [97]. This electrode exhibited a highly reversible capacity and fast charging and discharging capabilities. A high capacity of 785  $\text{mAh}/\text{g}$  was achieved at a rate of 1 C, which could be maintained without decaying up to 500 cycles. Moreover, a rate up to 60 C was also demonstrated, rendering a fast discharge potential.

Wu and coworkers used a 3D electrode of sulfur embedded in porous GSs in Li–S batteries [100]. The GSs worked as a framework that could provide a high electronic conductive network, the ability to absorb intermediate polysulfides, and mechanical support to accommodate the volume changes during the charge and discharge processes. As a result, the S-GS electrodes with 80 wt% sulfur could deliver a high areal specific capacity (4.53  $\text{mAh}/\text{cm}^2$  after 300 cycles) and a slow decay rate at 0.1 C (0.08% per cycle after 300 cycles). This is a significant step toward the application of Li–S batteries.

### Supercapacitors

3DGNs have been used as electrodes in both double-layer capacitors and pseudo-capacitors [7, 8, 28, 101–108]. Supercapacitor electrodes based on 3D hierarchical graphene/polypyrrole aerogels exhibit excellent electrochemical performance, including a high specific capacitance up to 253 F/g, a good rate performance and outstanding cycle stability [101]. Huang and coworkers used 3DGNs as the working electrode in a supercapacitor [103]. A capacitance of 341 F/g and an energy density of 16.2  $\text{Wh}/\text{kg}$  were measured in an alkali electrolyte, while the values were 166 F/g and

52.5 Wh/kg, respectively, in an organic electrolyte. Additionally, because of the high packing density of the 3DGNs, higher volumetric power densities of 20.7 and 67.2 Wh/L in alkali and organic electrolytes were obtained. After 1000 galvanostatic charge/discharge cycles, over 96 and 86% of the original capacitance could be retained in alkaline and organic electrolytes, respectively.

### Solar cells

3DGNs can be used as transparent conducting films or as the active material in solar cells [30]. In dye sensitized solar cells (DSSCs), 3DGNs prepared by CVD with a nickel foam rod as the template were added to the photoanode to boost the photovoltaic performance [109]. Even with a small amount of the 3DGN (0.2 wt%), the short-circuit current density and power conversion efficiency ( $\eta$ ) were improved, which was caused by the enhanced amount of dye absorption and the prolonged electron lifetime. Compared with that of a pure P25 photoanode-based DSSC, the  $\eta$  increased by 32.7% under AM-1.5G with the light intensity of one sun when a 3DGN (1 wt%)-P25 photoanode was adopted (from 4.96 to 6.58%). After optimizing the thickness of the added 3DGN layer, the  $\eta$  further increased to 6.87%.

### PERSPECTIVES

Much progress has been achieved on the synthesis and application of graphene/GO-based 3D frameworks. However, there are still some challenges to overcome. The first is the precise control of the 3DGN structures, including the growth of layers, the pore size and porosity. Most of the reported 3DGNs have a wide pore size distribution, ranging from one hundred to several hundreds of micrometers. Large pore sizes decrease the mechanical properties of the resulting materials. Thus, single-layered 3DGNs are hardly ever synthesized, owing to their fragile mechanical properties and large pore sizes. The fabrication of 3DGNs with uniform meso- or micropores and controlled layers are much needed. In template-assisted synthesis, the fabrication of a template with uniform meso- or micropores is important. In the assembly approach, gaining more control over the layer growth and size of the GO/graphene sheets will be helpful. The second challenge is to further improve the mechanical and electrical properties of the 3DGNs. Increasing and strengthening the cross-linking between the graphene/GO sheets by increasing the surface functional moieties or adding cross-linkers will improve the inter-sheet binding of the graphene/GO sheets and the mechanical and electrical properties. Thus, continued innovative

research and development is required to further improve the properties and applications of 3DGNs.

### FUNDING

This work was supported by the Ministry of Science and Technology of China (2011CB932602), the National Natural Science Foundation of China (50275093 and 51472124), the Ministry of Education (B12015) and the National Science Foundation of Tianjin City (10ZCGHHZ00600).

### REFERENCES

- Geim, AK. Graphene: status and prospects. *Science* 2009; **324**: 1530–4.
- Winzer, T, Knorr, A and Malic, E. Carrier multiplication in graphene. *Nano Lett* 2010; **10**: 4839.
- Li, T, Luo, L and Hupalo, M *et al.* Femtosecond population inversion and stimulated emission of dense Dirac fermions in graphene. *Phys Rev Lett* 2012; **108**: 167401.
- Cao, XH, Yin, ZY and Zhang, H. Three-dimensional graphene materials: preparation, structures and application in supercapacitors. *Energy Environ Sci* 2014; **7**: 1850–65.
- Nardecchia, S, Carriazo, D and Ferrer, ML *et al.* Three dimensional macroporous architectures and aerogels built of carbon nanotubes and/or graphene: synthesis and applications. *Chem Soc Rev* 2013; **42**: 794–830.
- Chabot, V, Higgins, D and Yu, AP *et al.* A review of graphene and graphene oxide sponge: material synthesis and applications to energy and the environment. *Energy Environ Sci* 2014; **7**: 1564–96.
- Li, C and Shi, G. Three-dimensional graphene architectures. *Nanoscale* 2012; **4**: 5549–63.
- Chen, Z, Ren, WC and Gao, L *et al.* Three-dimensional flexible and conductive interconnected graphene networks grown by chemical vapour deposition. *Nat Mater* 2011; **10**: 424–8.
- Xie, X, Zhou, YL and Bi, HC *et al.* Large-range control of the microstructures and properties of three-dimensional porous graphene. *Sci Rep* 2013; **3**: 2117.
- Bi, H, Xie, X and Yin, K *et al.* Spongy graphene as a highly efficient and recyclable sorbent for oils and organic solvents. *Adv Funct Mater* 2012; **22**: 4421–5.
- Zhang, XT, Sui, ZY and Xu, B *et al.* Mechanically strong and highly conductive graphene aerogel and its use as electrodes for electrochemical power sources. *J Mater Chem* 2011; **21**: 6494–7.
- Worsley, MA, Pauzauskie, PJ and Olson, TY *et al.* Synthesis of graphene aerogel with high electrical conductivity. *J Am Chem Soc* 2010; **132**: 14067–9.
- Yavari, F, Chen, Z and Thomas, AV *et al.* High sensitivity gas detection using a macroscopic three-dimensional graphene foam network. *Sci Rep* 2011; **1**: 166.
- Li, N, Chen, Z and Ren, WC *et al.* Flexible graphene-based lithium ion batteries with ultrafast charge and discharge rates. *Proc Natl Acad Sci U.S.A.* 2012; **109**: 17360–5.

15. Chen, Z, Xu, C and Ma, C *et al.* Lightweight and flexible graphene foam composites for high-performance electromagnetic interference shielding. *Adv Mater* 2013; **25**: 1296–300.
16. Pettes, MT, Ji, H and Ruoff, RS *et al.* Thermal transport in three-dimensional foam architectures of few-layer graphene and ultrathin graphite. *Nano Lett* 2012; **12**: 2959–64.
17. Xiao, X, Michael, JR and Beechem, T *et al.* Three dimensional nickel–graphene core–shell electrodes. *J Mater Chem* 2012; **22**: 23749–54.
18. Zhou, M, Lin, T and Huang, F *et al.* Highly conductive porous graphene/ceramic composites for heat transfer and thermal energy storage. *Adv Funct Mater* 2013; **23**: 2263–9.
19. Ning, G, Fan, Z and Wang, G *et al.* Gram-scale synthesis of nanomesh graphene with high surface area and its application in supercapacitor electrodes. *Chem Commun* 2011; **47**: 5976–8.
20. Mecklenburg, M, Schuchardt, A and Mishra, YK *et al.* Aerographite: ultra lightweight, flexible nanowall, carbon microtube material with outstanding mechanical performance. *Adv Mater* 2012; **24**: 3486–90.
21. Wang, R, Hao, Y and Wang, Z. Large-diameter graphene nanotubes synthesized using Ni nanowire templates. *Nano Lett* 2010; **10**: 4844–50.
22. Yoon, SM, Choi, WM and Baik, H *et al.* Synthesis of multilayer graphene balls by carbon segregation from nickel nanoparticles. *ACS Nano* 2012; **6**: 6803–11.
23. Ito, Y, Tanabe, Y and Qiu, HJ, *et al.* High-quality three-dimensional nanoporous graphene. *Angew Chem Int Ed* 2014; **53**: 4822–6.
24. Lee, JS, Ahn, HJ and Yoon, JC *et al.* Three-dimensional nano-foam of few-layer graphene grown by CVD for DSSC. *Phys Chem Chem Phys* 2012; **14**: 7938–43.
25. Li, W, Gao, S and Wu, L *et al.* High-density three-dimension graphene macroscopic objects for high-capacity removal of heavy metal ions. *Sci Rep* 2013; **3**: 2125.
26. Cao, X, Shi, Y and Shi, W *et al.* Preparation of novel 3D graphene networks for supercapacitor applications. *Small* 2011; **7**: 3163–8.
27. Liu, ZC, Tu, ZQ and Lin, YF *et al.* Synthesis of three-dimensional graphene from petroleum asphalt by chemical vapor deposition. *Mater Lett* 2014; **122**: 285–8.
28. Dong, X, Wang, X and Wang, L *et al.* 3D graphene foam as a monolithic and macroporous carbon electrode for electrochemical sensing. *ACS Appl Mater Interfaces* 2012; **4**: 3129–33.
29. Dong, X, Wang, X and Wang, L *et al.* Synthesis of a MnO<sub>2</sub>–graphene foam hybrid with controlled MnO<sub>2</sub> particle shape and its use as a supercapacitor electrode. *Carbon* 2012; **50**: 4865–70.
30. Bi, H, Huang, F and Liang, J *et al.* Large-scale preparation of highly conductive three dimensional graphene and its applications in CdTe solar cells. *J Mater Chem* 2011; **21**: 17366–70.
31. Pettes, MT, Li, H and Ruoff, RS *et al.* Thermal transport in three-dimensional foam architectures of few-layer graphene and ultrathin graphite. *Nano Lett* 2012; **12**: 2959–64.
32. Bo, Z, Yu, KH and Lu, G *et al.* Understanding growth of carbon nanowalls at atmospheric pressure using normal glow discharge plasma-enhanced chemical vapor deposition. *Carbon* 2011; **49**: 1849–58.
33. Yu, KH, Wang, P and Lu, G *et al.* Patterning vertically oriented graphene sheets for nanodevice applications. *J Phys Chem Lett* 2011; **2**: 537–42.
34. Mao, S, Yu, KH and Chang, JB *et al.* Direct growth of vertically-oriented graphene for field-effect transistor biosensor. *Sci Rep* 2013; **3**: 1696.
35. Wang, XB, Zhang, YJ and Zhi, CY *et al.* Three-dimensional strutted graphene grown by substrate-free sugar blowing for high-power-density supercapacitors. *Nat Commun* 2013; **4**: 2905.
36. Bai, H, Li, C and Wang, X *et al.* On the gelation of graphene oxide. *J Phys Chem C* 2011; **115**: 5545–51.
37. Bai, H, Li, C and Wang, X *et al.* A pH-sensitive graphene oxide composite hydrogel. *Chem Commun* 2010; **46**: 2376–8.
38. Compton, OC, An, Z and Putz, KW *et al.* Additive-free hydrogelation of graphene oxide by ultrasonication. *Carbon* 2012; **50**: 3399–406.
39. Chen, W and Yan, L. *In situ* self-assembly of mild chemical reduction graphene for three-dimensional architectures. *Nanoscale* 2011; **3**: 3132–7.
40. Sheng, KX, Xu, YX and Li, C *et al.* High-performance self-assembled graphene hydrogels prepared by chemical reduction of graphene oxide. *New Carbon Mater* 2011; **26**: 9–15.
41. Sheng, KX, Sun, YQ and Li, C *et al.* Ultrahigh-rate supercapacitors based on electrochemically reduced graphene oxide for ac line-filtering. *Sci Rep* 2012; **2**: 247.
42. Li, Y, Sheng, K and Yuan, W *et al.* A high-performance flexible fibre-shaped electrochemical capacitor based on electrochemically reduced graphene oxide. *Chem Commun* 2013; **49**: 291–3.
43. Xu, Y, Sheng, K and Li, C *et al.* Self-assembled graphene hydrogel via a one-step hydrothermal process. *ACS Nano* 2010; **4**: 4324–30.
44. Tang, Z, Shen, S and Zhuang, J *et al.* Noble-metal-promoted three-dimensional macroassembly of single-layered graphene oxide. *Angew Chem Int Ed* 2010; **49**: 4603–7.
45. Wei, W, Yang, S and Zhou, H *et al.* 3D graphene foams cross-linked with pre-encapsulated Fe<sub>3</sub>O<sub>4</sub> nanospheres for enhanced lithium storage. *Adv Mater* 2013; **25**: 2909–14.
46. Su, Y, Zhang, Y and Zhuang, X *et al.* Low-temperature synthesis of nitrogen/sulfur co-doped three-dimensional graphene frameworks as efficient metal-free electrocatalyst for oxygen reduction reaction. *Carbon* 2013; **62**: 296–301.
47. Han, Z, Tang, Z and Li, P *et al.* Ammonia solution strengthened three-dimensional macro-porous graphene aerogel. *Nanoscale* 2013; **5**: 5462–7.
48. Tao, Y, Xie, X and Lv, W *et al.* Towards ultrahigh volumetric capacitance: graphene derived highly dense but porous carbons for supercapacitors. *Sci Rep* 2013; **3**: 2975.
49. Cong, HP, Ren, XC and Wang, P *et al.* Macroscopic multifunctional graphene-based hydrogels and aerogels by a metal ion induced self-assembly process. *ACS Nano* 2012; **6**: 2693–703.
50. Chen, H, Muller, MB and Gilmore, KJ *et al.* Mechanically strong, electrically conductive, and biocompatible graphene paper. *Adv Mater* 2008; **20**: 3557–61.
51. Chen, CM, Yang, QH and Yang, YG *et al.* Self-assembled free-standing graphite oxide membrane. *Adv Mater* 2009; **21**: 3007–11.
52. Li, X, Zhang, G and Bai, X *et al.* Highly conducting graphene sheets and Langmuir–Blodgett films. *Nat Nanotechnol* 2008; **3**: 538–42.
53. Shen, JF, Hu, YZ and Li, C *et al.* Layer-by-layer self-assembly of graphene nanoplatelets. *Langmuir* 2009; **25**: 6122–8.
54. Ahn, H, Kim, H and Kim, JM *et al.* Controllable pore size of three dimensional self-assembled foam-like graphene and its wettability. *Carbon* 2013; **64**: 27–34.
55. Hu, H, Zhao, ZB and Wan, WB *et al.* Ultralight and highly compressible graphene aerogels. *Adv Mater* 2013; **25**: 2219–23.
56. Hu, CG, Zhai, XQ and Liu, LL *et al.* Spontaneous reduction and assembly of graphene oxide into three-dimensional graphene network on arbitrary conductive substrates. *Sci Rep* 2013; **3**: 2065.
57. Choi, BG, Yang, M and Hong, WH *et al.* 3D macroporous graphene frameworks for supercapacitors with high energy and power densities. *ACS Nano* 2012; **6**: 4020–8.

58. Huang, X, Qian, K and Yang, J *et al.* Functional nanoporous graphene foams with controlled pore sizes. *Adv Mater* 2012; **24**: 4419–23.
59. Yao, HB, Ge, J and Wang, CF *et al.* A flexible and highly pressure-sensitive graphene-polyurethane sponge based on fractured microstructure design. *Adv Mater* 2013; **25**: 6692–8.
60. Estevez, L, Kellarakis, A and Gong, Q *et al.* Multifunctional graphene/platinum/naion hybrids via ice templating. *J Am Chem Soc* 2011; **133**: 6122–5.
61. Yu, G, Hu, L and Vosgueritchian, M *et al.* Solution-processed graphene/MnO<sub>2</sub> nanostructured textiles for high-performance electrochemical capacitors. *Nano Lett* 2011; **11**: 2905–11.
62. Xu, Y, Wu, Q and Sun, Y *et al.* Three-dimensional self-assembly of graphene oxide and DNA into multifunctional hydrogels. *ACS Nano* 2010; **4**: 7358–62.
63. Sun, S and Wu, P. A one-step strategy for thermal- and pH-responsive graphene oxide interpenetrating polymer hydrogel networks. *J Mater Chem* 2011; **21**: 4095–7.
64. Luan, VH, Tien, HN and Hoa, LT *et al.* Synthesis of a highly conductive and large surface area graphene oxide hydrogel and its use in a supercapacitor. *J Mater Chem A* 2013; **1**: 208–11.
65. Luan, VH, Chung, JS and Kim, EJ *et al.* The molecular level control of three-dimensional graphene oxide hydrogel structure by using various diamines. *Chem Eng J* 2014; **246**: 64–70.
66. Sudeep, PM, Narayanan, TN and Ganesan, A *et al.* Covalently interconnected three-dimensional graphene oxide solids. *ACS Nano* 2013; **7**: 7034–40.
67. Zhao, Y, Liu, J and Hu, Y *et al.* Highly compression-tolerant supercapacitor based on polypyrrole-mediated graphene foam electrodes. *Adv Mater* 2013; **25**: 591–5.
68. Chen, XJ, Eggers, PK and Slattery, AD *et al.* Template-free assembly of three-dimensional networks of graphene hollow spheres at the water/toluene interface. *J Colloid Interface Sci* 2014; **30**: 174–7.
69. Haag, DR and Kung, HH. Metal free graphene based catalysts: a review. *Top Catal* 2014; **57**: 762–73.
70. Machadoab, BF and Serp, P. Graphene-based materials for catalysis. *Catal Sci Technol* 2012; **2**: 54–75.
71. Huang, CC, Li, C and Shi, GQ. Graphene based catalysts. *Energy Environ Sci* 2012; **5**: 8848–68.
72. Scheuermann, GM, Rumi, L and Steurer, P *et al.* Palladium nanoparticles on graphite oxide and its functionalized graphene derivatives as highly active catalysts for the Suzuki–Miyaura coupling reaction. *J Am Chem Soc* 2009; **131**: 8262–70.
73. Zhang, N, Zhang, Y and Pan, X *et al.* Constructing ternary CdS–graphene–TiO<sub>2</sub> hybrids on the flatland of graphene oxide with enhanced visible-light photoactivity for selective transformation. *J Phys Chem C* 2012; **116**: 18023–31.
74. Gonçalves, GAB, Pires, SMG and Simoes, MMQ *et al.* Three-dimensional graphene oxide: a promising green and sustainable catalyst for oxidation reactions at room temperature. *Chem Commun* 2014; **50**: 7673–6.
75. Zhang, YJ, Chu, M and Yang, L *et al.* Synthesis and oxygen reduction properties of three-dimensional sulfur-doped graphene networks. *Chem Commun* 2014; **50**: 6382–5.
76. Xue, YH, Yu, DS and Dai, LM *et al.* Three-dimensional B, N-doped graphene foam as a metal-free catalyst for oxygen reduction reaction. *Phys Chem Chem Phys* 2013; **15**: 12220–6.
77. Han, WJ, Ren, L and Gong, LJ *et al.* Self-assembled three-dimensional graphene-based aerogel with embedded multifarious functional nanoparticles and its excellent photoelectrochemical activities. *ACS Sustain Chem Eng* 2014; **2**: 741–8.
78. Wu, ZS, Yang, S and Sun, Y *et al.* 3D nitrogen-doped graphene aerogel-supported Fe<sub>3</sub>O<sub>4</sub> nanoparticles as efficient electrocatalysts for the oxygen reduction reaction. *J Am Chem Soc* 2012; **134**: 9082–5.
79. Kung, CC, Lin, PY and Xue, YH *et al.* Three dimensional graphene foam supported platinum-ruthenium bimetallic nanocatalysts for direct methanol and direct ethanol fuel cell applications. *J Power Sources* 2014; **256**: 329–35.
80. Mahyari, M, Laeini, MS and Shaabani, A. Aqueous aerobic oxidation of alkyl arenes and alcohols catalyzed by copper(II) phthalocyanine supported on three-dimensional nitrogen-doped graphene at room temperature. *Chem Commun* 2014; **50**: 7855–7.
81. Hu, CG, Zhai, XQ and Zhao, Y *et al.* Small-sized PdCu nanocapsules on 3D graphene for high-performance ethanol oxidation. *Nanoscale* 2014; **6**: 2768–75.
82. Hu, CG, Cheng, HH and Zhao, Y *et al.* Newly-designed complex ternary Pt/PdCu nanoboxes anchored on three-dimensional graphene framework for highly efficient ethanol oxidation. *Adv Mater* 2012; **24**: 5493–8.
83. Lei, YL, Chen, F and Luo, Y *et al.* Synthesis of three-dimensional graphene oxide foam for the removal of heavy metal ions. *Chem Phys Lett* 2014; **593**: 122–7.
84. Ai, L and Jiang, J. Removal of methylene blue from aqueous solution with self-assembled cylindrical graphene–carbon nanotube hybrid. *Chem Eng J* 2012; **192**: 156–63.
85. Xu, Y, Wu, Q and Sun, Y *et al.* Three-dimensional self-assembly of graphene oxide and DNA into multifunctional hydrogels. *ACS Nano* 2010; **4**: 7358–62.
86. Brownson, DAC, Figueiredo-Filho, LCS and Ji, XB *et al.* Freestanding three-dimensional graphene foam gives rise to beneficial electrochemical signatures within non-aqueous media. *J Mater Chem A* 2013; **1**: 5962.
87. Dong, X, Chen, J and Ma, Y *et al.* Super hydrophobic and superoleophilic hybrid foam of graphene and carbon nanotube for selective removal of oils or organic solvents from the surface of water. *Chem Commun* 2012; **48**: 10660–2.
88. Sun, H, Xu, Z and Gao, C. Multifunctional, ultra-flyweight, synergistically assembled carbon aerogels. *Adv Mater* 2013; **25**: 2554–60.
89. Mecklenburg, M, Schuchardt, A and Mishra, YK *et al.* Aerographite: ultra lightweight, flexible nanowall, carbon microtube material with outstanding mechanical performance. *Adv Mater* 2012; **24**: 3486–90.
90. Lei, LL, Chen, F and Luo, YJ *et al.* Three-dimensional magnetic graphene oxide foam/Fe<sub>3</sub>O<sub>4</sub> nanocomposite as an efficient absorbent for Cr(VI) removal. *J Mater Sci* 2014; **49**: 4236–5.
91. Ma, Y, Zhao, MG and Cai, B *et al.* 3D graphene foams decorated by CuO nanoflowers for ultrasensitive ascorbic acid detection. *Biosens Bioelectron* 2014; **59**: 384–8.
92. Crowder, SW, Prasai, D and Rath, R *et al.* Three-dimensional graphene foams promote osteogenic differentiation of human mesenchymal stem cells. *Nanoscale* 2013; **5**: 4171–6.
93. Song, Q, Jiang, Z and Li, N *et al.* Anti-inflammatory effects of three-dimensional graphene foams cultured with microglial cells. *Biomaterials* 2014; **35**: 6930–40.
94. Kim, BJ, Yang, G and Park, MJ *et al.* Three-dimensional graphene foam-based transparent conductive electrodes in GaN-based blue light-emitting diodes. *Appl Phys Lett* 2013; **102**: 161902.
95. Biener, J, Stadermann, M and Suss, M *et al.* Advanced carbon aerogels for energy applications. *Energy Environ Sci* 2011; **4**: 656–67.
96. Chen, WF, Huang, YX and Li, DB *et al.* Preparation of a macroporous flexible three dimensional graphene sponge using an ice template as the anode material for microbial fuel cells. *RSC Adv* 2014; **4**: 21619–24.

97. Luo, JS, Liu, JL and Zeng, ZY *et al.* Three-dimensional graphene foam supported Fe<sub>3</sub>O<sub>4</sub> lithium battery anodes with long cycle life and high rate capability. *Nano Lett* 2013; **13**: 6136–43.
98. Yang, Y, Fan, XJ and Casillas, G *et al.* Three-dimensional nanoporous Fe<sub>2</sub>O<sub>3</sub>/Fe<sub>3</sub>C-graphene heterogeneous thin films for lithium-ion batteries. *ACS Nano* 2014; **8**: 3939–46.
99. Zhou, GM. Fibrous hybrid of graphene and sulfur nanocrystals for high-performance lithium-sulfur batteries. *ACS Nano* 2013; **7**: 5367–75.
100. Lu, ST, Chen, Y and Wu, XH *et al.* Three-dimensional sulfur/graphene multi-functional hybrid sponges for lithium-sulfur batteries with large areal mass loading. *Sci Rep* 2014; **4**: 4629.
101. Ye, SB and Feng, JC. Self-assembled three-dimensional hierarchical graphene/polypyrrole nanotube hybrid aerogel and its application for supercapacitors. *ACS Appl Mater Interfaces* 2014; **6**: 9671–9.
102. Chen, J, Li, C and Shi, G. Graphene materials for electrochemical capacitors. *J Phys Chem Lett* 2013; **4**: 1244–53.
103. Yuan, CZ, Zhou, L and Hou, LR. Facile fabrication of self-supported three-dimensional porous reduced graphene oxide film for electrochemical capacitors. *Mater Lett* 2014; **124**: 253–5.
104. Hu, J, Kang, Z and Fei, Li *et al.* Graphene with three-dimensional architecture for high performance supercapacitor. *Carbon* 2014; **67**: 221–9.
105. Chen, J, Sheng, KX and Luo, PH *et al.* Graphene hydrogels deposited in nickel foams for high-rate electrochemical capacitors. *Adv Mater* 2012; **24**: 4569–73.
106. Jiang, H, Lee, PS and Li, CZ. 3D carbon based nanostructures for advanced supercapacitors. *Energy Environ Sci* 2013; **6**: 41–53.
107. Zhao, Y, Liu, J and Hu, Y *et al.* Highly compression-tolerant supercapacitor based on polypyrrole-mediated graphene foam electrodes. *Adv Mater* 2013; **25**: 591–5.
108. Zhang, XT, Sui, ZY and Xu, B *et al.* Mechanically strong and highly conductive graphene aerogel and its use as electrodes for electrochemical power sources. *J Mater Chem* 2011; **21**: 6494–7.
109. Tang, B, Hu, GX and Gao, HY *et al.* Three-dimensional graphene network assisted high performance dye sensitized solar cells. *J Power Sources* 2013; **234**: 60–8.